NIST Technical Note 1525

The NIST 30/60 MHz Tuned Radiometer for Noise Temperature Measurements

Chriss A. Grosvenor
Robert L. Billinger
Radio-Frequency Technology Division
Electronics and Electrical Engineering Laboratory

May 2002

U.S. Department of Commerce
Donald L. Evans, Secretary

Technology Administration
Phillip J. Bond. Under Secretary of Commerce for Technology

National Institute of Standards and Technology
Arden L. Bement, Jr., Director

Certain commercial entities, equipment, or materials may be identified in this document in order to describe an experimental procedure or concept adequately. Such identification is not intended to imply recommendation or endorsement by the National Institute of Standards and Technology, nor is it intended to imply that the entities, materials, or equipment are necessarily the best available for the purpose.

National Institute of Standards and Technology Technical Note 1525
Natl. Inst. Stand. Technol. Tech. Note 1525, 33 pages (May 2002)
CODEN: NTNOEF

U.S. GOVERNMENT PRINTING OFFICE
WASHINGTON: 2002

For sale by the Superintendent of Documents, U.S. Government Printing Office
Internet: bookstore.gpo.gov Phone: (202) 512-1800 Fax: (202) 512-2250
Mail: Stop SSOP, Washington, DC 20402-0001

CONTENTS

The NIST 30/60 MHz Tuned Radiometer for Noise Temperature Measurements

Chriss A. Grosvenor
Robert L. Billinger

Radio-Frequency Technology Division
Electronics and Electrical Engineering Laboratory
National Institute of Standards and Technology
Boulder, CO 80305-3328

The NIST Noise project has completed reconstruction of its 30/60 MHz tuned, coaxial (Type N) radiometer system. This system is used at low frequencies, where isolators are impractical to incorporate. Without isolators, the ambient and cryogenic standards are tuned to the impedance of the device under test to minimize mismatches. Although this system had existed prior to publication of this technical note, enough modifications and improvements have been made to warrant a new report. This note will briefly review the original system, and discuss the theory as well as the design, testing, and capabilities of the present system. A more detailed uncertainty analysis, as well as details of system troubleshooting, are also included.

Key Words: noise; noise measurement; noise temperature; radiometer; thermal noise

1. INTRODUCTION

The new tuned radiometer system is an improvement on the original radiometer first described in an National Bureau of Standards (NBS) internal report written in 1981 [1]. Most of the original control hardware has been replaced and newer software has been incorporated. The system has also been mounted in a measurement rack (see Figure 1) so that the system temperature can be more tightly controlled and its mechanical stability improved.

Most of the radiometers in use by the National Institute of Standards and Technology (NIST) [2, 3] are isolated radiometers with 40 to 60 dB of impedance isolation, thus minimizing the effect of any change in source impedance. Below about 1 GHz, however, the isolators

become impractically large to incorporate and another approach is required. Without an isolator in the measurement path, the radiometer is sensitive to a change in source impedance from one standard or device to the next. However, in the 30/60 MHz system design, isolation is unnecessary because the cryogenic and ambient standards are tuned to the impedance of the device under test (DUT), thus creating a reflectionless load.

One difference between a tuned system and other measurement systems is that the reflection coefficient Γ of the system, the devices, and the standards does not need to be known. Because everything is matched to the impedance of the DUT, mismatch and asymmetry ratios are taken to be unity. A disadvantage of this system is that the impedance of the standards, although tuned to the DUT and measured, can still lead to small mismatch and asymmetry errors, which become the largest source of uncertainty. However, due to the simplicity of the system, we have found that measurements are easily accomplished and tend to be very stable and repeatable from year to year.

Section 2 explains the theory behind this system, Section 3 discusses the design, and Section 4 presents the testing, measurements, and comparisons. Section 5 covers the uncertainty analysis for this system, and Section 6 is reserved for a brief summary. Appendix A is describes how to troubleshoot the present system.

2. THEORETICAL BACKGROUND

This section explains the basic theoretical equations used to derive the noise temperature of the DUT. The theory is described in more detail in reference [3].

We assume that our radiometer systems are linear; therefore, we can determine the noise temperature of an unknown device by measuring the output power of the DUT and two known standards. We then fit these data to a straight line. The two known standards have well-characterized temperatures. The two standards are: (1) an ambient standard that is maintained at room temperature, and (2) the cryogenic standard with a physical temperature of about 77 K (the boiling point of liquid nitrogen). The temperatures and powers can be used to calculate the noise temperature of the DUT by use of the following radiometer equation [4, 5],

$$T_x = T_a + (T_s - T_a)\frac{Y_x - 1}{Y_s - 1}\frac{M_s \eta_s}{M_x \eta_x}. \quad (1)$$

The subscript x refers to the unknown device, subscript s refers to the cryogenic standard, and subscript a refers to the ambient standard, symbol T denotes temperature, M the mismatch, η the efficiency, and Y the power ratio, where Y_x is the power ratio of the unknown DUT relative to the ambient standard and Y_s is the power ratio of the cryogenic standard relative to the ambient standard.

Figure 2 shows a typical measurement setup. The box with an arrow denotes the isolator in a typical radiometer. However, there is no isolator in the 30/60 MHz system so the first component before the radiometer is a preamplifier. The effects of this will be discussed in Section 3.

In any power-measurement system, the power available to a load is not the same as the power delivered to the load because of reflective interfaces and path losses. The two mechanisms limiting the power are the ratio of mismatch factors and path asymmetries. The first

$$M = \frac{(1-|\Gamma_g|^2)(1-|\Gamma_L|^2)}{|1-\Gamma_g\Gamma_L|^2}, \quad (2)$$

mechanism is the mismatch factor,

where Γ_g and Γ_L are the reflection coefficients to the left and right of the discontinuity, as shown in Figure 3. The mismatch between any two ports does not equal unity, but since all devices are tuned to the same impedance and the switches are measured and found to be nearly identical, the ratio of mismatches becomes very nearly unity. The uncertainty comes into play when we actually measure the reflection coefficients with a vector impedance meter.

The mechanism is the ratio of path efficiencies (asymmetry) between measurement paths and also limits the amount of power delivered to the radiometer. The efficiency depends on the

path loss S_{21} from the source at planes 1, 2, or 3, to the load (or radiometer) at plane 0, (see Figure 2):

$$\eta = \frac{|S_{21}|^2}{|1 - S_{11}|^2}. \tag{3}$$

Equation (3) assumes a reflectionless load. For our system, the only path differences would be due to the switch that connects between the DUT, cryogenic standard, and ambient standard, since the cable to the first amplifier is the same in all three cases. Since the switches are electrically identical in either direction, the ratio of efficiencies is nearly unity. For our system, the measured efficiencies were found to be equal to within 0.000237, which is less than the measurement uncertainty and will be discussed in section 5.

Because the ambient standard, cryogenic standard, and DUT all have the same impedance,

$$T_x = T_a + (T_s - T_a)\frac{Y_x - 1}{Y_s - 1}. \tag{4}$$

the ratios of mismatches and efficiencies in eq (1) are set equal to one and the radiometer equation reduces to

3. DESIGN, CONSTRUCTION, AND OPERATION

3.1 Description of Measurement System

Figure 4 is a schematic diagram for the present measurement system. A radiometer is basically a receiver and is designed to amplify a noise signal to a level that can be measured by a NIST Type-IV power meter [6].

The DUT and/or standards are connected to the Type-N ports of two coaxial switches. These two switches are then connected to a third switch that is followed by a preamplifier having approximately 35 dB of gain. The signal is then fed into either a 30 MHz or a 60 MHz filter having respective bandwidths of 0.77 MHz or 1.38 MHz. A variable attenuator, used to test the

linearity of the intermediate frequency (IF) section, has been included at this point. The attenuator can be switched from 0 to 12 dB depending on the frequency and noise temperature of the DUT. The 5 dB attenuator that follows provides isolation into the next amplifier having 30 dB of gain. There is a level-set attenuator that allows the overall system signal level to be set depending on the approximate noise temperature of the DUT. Since we measure devices with noise temperatures ranging from 9000 K to 10,000 K we do not need to adjust the level-set attenuator once it has been set. The next 5 dB attenuator again provides isolation into another 30 dB-gain amplifier. A 6 dB attenuator follows, that provides impedance matching into the last 30 dB-gain amplifier. At this point, the signal is either switched into a 50 Ω load for power-off measurements, or into a 200 Ω bolometer for measurement with a digital voltmeter (DVM) and a Type-IV power meter [6]. All of the components that follow the filters are mounted on a water-cooled brass plate used to maintain the overall system temperature. The preamplifier and switches prior to the filters sit on a separate water-cooled plate at the base of the cabinet (see Figure 1).

The noise source is either a DUT, a cryogenic standard, or an ambient standard. The DUT is typically a noise diode generating an output noise temperature between 9500 K and 11,000 K. The ambient standard is a load submersed in an oil bath at room temperature. The oil bath and the design of the Dewar ensure minimal temperature changes, giving a stable noise power output [1]. The load temperature is measured with a thermometer immersed in the oil bath. The cryogenic standard is similar to the ambient standard except that the load is now immersed in a bath of liquid nitrogen. To determine the boiling point of liquid nitrogen, the atmospheric pressure is measured and substituted into the vapor-pressure equation. The physical temperature of the load is assumed to be at the same temperature as the liquid nitrogen, and a small temperature correction is made to account for the losses along the coaxial lines and adapters. A final noise temperature is obtained at the output port of the standard. Both standards have tunable GR900 output ports that are connected to the Type-N ports of the switches through 14 mm coaxial airlines and adapters. The noise power of each device is measured using a low-band thermistor mount in combination with a NIST Type-IV power meter card and a DVM.

3.2 Measurement Sequence

A test of the customer's device consists of the following sequence:

(1) An impedance meter is calibrated using a one-port calibration measurement [7].

(2) The impedance of the DUT is measured, stored, and later converted to a reflection coefficient Γ by means of the following equation:

$$\Gamma = \frac{Z_{meas} - Z_0}{Z_{meas} + Z_0}, \tag{5}$$

where $Z_0 = 50\ \Omega$ and Z_{meas} may be complex.

(3) The ambient and cryogenic standards are tuned until their impedances are the same as the DUT.

(4) The DUT is then connected to port 3, the cryogenic standard to port 2, and the ambient standard to port 4.

(5) The program controls switches to various RF paths used to supply power to the pre-amplifier, and the measurement sequence begins.

(6) The output power is measured for the DUT, the ambient standard and the cryogenic standard [6]. From these powers, a noise temperature is computed for the DUT. This sequence is repeated for a total of 25 measurements.

(7) After the first 25 measurements, the operator reduces the attenuation by 3 dB, doubling the output power.

(8) At the end of 50 measurements, the raw powers, temperatures, and uncertainties are stored in a measurement file.

For this test, a reference or check standard is measured once according to the above sequence, and the customer's device is measured a total of three times.

4. TESTING

4.1 Primary Standards

Figure 5 is a photograph of the ambient (right) and cryogenic (left) noise standards. The ambient standard is a load enclosed in a metal housing that is in turn encased in an outer housing.

The inner housing contains the capacitor-plate tuning structure; all of this is immersed in mineral oil. The temperature of the ambient standard is read directly by a thermometer inserted into the inner housing. This standard was originally designed to be used as a hot standard. Power can be supplied to eight power resistors located at the bottom of the inner housing. The resistors are used to heat the oil to a known, controlled temperature. The ambient standard is able to maintain its temperature to within 0.05 K over an 8 h period.

The cryogenic standard also uses a load, but the housing is now immersed in liquid nitrogen. The capacitor-plate tuning structure for this standard is the same. The output temperature of the cryogenic standard, which is calculated by the program, depends on the barometric pressure in the laboratory. Both standards use GR900 precision airlines, connectors, and adapters for the transition from the standard to the measurement ports.

4.2 Stability

One of the most important features of any radiometric system is its ability to remain stable over a measurement period. This includes temperature stability, the stability of the power measurement, and the stability of the other measurement equipment used by the system. Stability in this sense is defined as small variations during the measurement period.

As mentioned previously, the ambient standard is able to maintain temperature to within 0.05 K over an 8 h period. Because of its stable thermal properties, the cryogenic standard's design requires only one refill per day of liquid nitrogen. Both standards are stable over the course of a complete measurement.

We need to determine the power stability of this system because the measured power is a direct measurement of the noise temperature of a DUT. In our system, there are two components that "measure" the noise temperature of a DUT. The first is the digital multimeter, and the second is a Type-IV power meter that includes a bolometer. When we looked at the power stability of our system, we first looked at the variations in readings coming from the digital multimeter. We found that these measurements were accurate to within 3 parts in 2000. Because NIST is heavily involved in power measurements, the accuracies of the bolometers are well known.

In this system, the impedance of the standards must be matched to that of the DUT accurately. The precision of the measurement is useful when we want to know the DUT's

available noise temperature and standard deviation. The vector impedance meter used for this particular system is not as precise as newer models, and therefore it is calibrated to improve precision. The uncertainty analysis, covered in the next section, explains the measurements we used to determine both the accuracy and precision of our measurements.

4.3 Linearity

All radiometers use amplifiers to amplify a signal, which is typically in the nanowatt range, into the milliwatt range so that a detector can accurately measure the signal. However, amplifiers can become nonlinear if overdriven by the input signal. Our use of the radiometer equation to calculate a DUT's noise temperature is justified by the fact that we have a linear system.

We check the linearity of the system by measuring 25 sets of noise powers. A set consists of Type-IV power-meter card measurements with no power supplied to it (power off); these provide the baseline reading [6]. Power is then supplied to the card, and we measure the cryogenic standard, the ambient standard, and the check standard or DUT. Then, 3 dB of attenuation is removed from the path (see Figure 4) and another set of 25 measurements is taken. The two resulting noise temperatures are compared and, if they agree to within 0.2 %, we may conclude that the system is linear.

4.4 Measurement and Comparison

The final tests on the system were to measure various check standards with known histories and compare current measurements with those taken approximately two years ago. Typically the criterion for satisfactory comparison is that the measured noise temperatures be within 50 K of previous results and have standard deviations of around 20 K. Figures 6 and 7 compare measurement results at 30 MHz and 60 MHz to past measurements. Figure 6 shows a measurement of the Type-N check standard X13BHZ.617. The historical measurement results at 30 MHz have an average temperature of 10136 K and a spread of 36 K. The most recent results at 30 MHz have an average temperature of 10116 K, and a spread of 19 K. The historical average at 60 MHz is 10180 K, compared to the recent average of 10185 K. The difference in noise temperatures between the historical and current average is 20 K. Data on another Type-N

check standard X13BHZ.817 are shown in figure 7. Historical data for this device exist only at 60 MHz. At that frequency the historical average is 9587 K and the recent average is 9570 K. This is a difference of 17 K.

We have made measurements using other connectors as well, and based on the criterion given above we have determined that the system is operating correctly.

5. UNCERTAINTY ANALYSIS

5.1 Background

The uncertainty analysis will follow the analysis as outlined in previous technical notes for total-power radiometers. The notation is consistent with that found in references [3], [8], and [9]. The standard uncertainty in the measurement of T_x is denoted by u_{Tx}. The combined standard uncertainty is composed of Type-A and Type-B uncertainties. The Type-A uncertainty is calculated as the standard deviation of the mean of several independent measurements of the quantity of interest. The first part of this section will deal with type-B uncertainties; type-A uncertainties are treated at the end of this section. We use $\mathscr{E}$ to denote the fractional standard uncertainty in a parameter; for example, $\mathscr{E}_{cry} = u_{TCry}/T_{cry}$. The contribution of the uncertainty in a particular parameter (e.g., T_{Cry}) to the uncertainty in T_x will be denoted u_{Tx}(Cry).

The noise temperature of a measured device is determined by the radiometer equation (1). Uncertainties in T_x arise due to uncertainties in the determination of the quantities appearing on the right side of eq (1). For quantities appearing in eq (1), the propagation of uncertainties is treated in the manner outlined in reference [10]. We will treat the following contributions to the uncertainty in T_x : the cryogenic standard, the ambient standard, lack of isolation, broadband mismatch effects, nonlinearity effects, the power ratio measurements, connector repeatability, and the errors introduced due to imperfect matching between ports and the asymmetry in the switches.

5.2 Primary Standards

The cryogenic standard contributes to the uncertainty in T_x as

$$\frac{u_{T_x}(Cry)}{T_x} = \left|1 - \frac{T_a}{T_x}\right| \left|\frac{T_s}{T_a - T_s}\right| \mathscr{E}_{Cry}. \tag{5}$$

The uncertainty attributed to the cryogenic standard is 0.22 K at 30 MHz and 0.28 K at 60 MHz so that its fractional uncertainty is 0.29 % and 0.37 %, respectively [1]. These numbers are based on a typical 10,000 K source.

The contribution of the uncertainty in the ambient standard temperature to that in the DUT noise temperature is given by

$$\frac{u_{T_x}(amb)}{T_x} = \left|\frac{T_x - T_s}{T_a - T_s}\right| \frac{T_a}{T_x} \mathscr{E}_{T_a}. \tag{6}$$

The ambient standard's physical temperature is measured with a calibrated thermometer. A conservative estimate of the uncertainty in the temperature measurement is $u_{Ta} = 0.1$ K or $\mathscr{E}_{Ta} =$ 0.034 %.

5.3 Mismatch Factors

Mismatch factors and efficiencies are not currently used in the radiometer equation because their ratios are close to unity; nonetheless, we still calculate their uncertainty. There will always be some mismatch between the DUT and the standards due to imperfections in the measurement software and the switching between ports, which cannot give repeatable results. The sections below describe how these values are obtained.

The ratio of mismatch factors contributes to the uncertainty in the DUT noise temperature according to

$$\frac{u_{T_x}(M/M)}{T_x} = \left|1 - \frac{T_a}{T_x}\right| \mathscr{E}_{M/M} \approx \left|1 - \frac{T_a}{T_x}\right| u_{M/M}. \tag{7}$$

The mismatch uncertainty depends strongly on the impedance measured by our vector impedance

meter. This means that the uncertainty analysis of the mismatch factor determined in the Technical Note for NFRad [3] is invalid, since a vector impedance meter is not used in the NFRad system. Deriving the uncertainty from an analytical point of view is complicated, so we used a Monte Carlo simulation to determine the uncertainty in the mismatch factor for the 30/60 MHz system.

The impedance of a device was measured on port 1, then moved to port 3 and measured, and then to port 4. This sequence was repeated for a total of five measurements. This was completed at both frequencies. The mean and standard deviation of these measurements were calculated and used as the random Type-A source of uncertainty for the mismatch. To determine the systematic Type-B uncertainty for this specific impedance meter, several NIST impedance standards were measured on the same vector impedance meter. The largest deviation was used for the systematic error in the Monte Carlo simulation. The random and systematic uncertainties were combined using root sum of squares to determine the overall uncertainties for the real and imaginary parts at 30 and 60 MHz. To find the total mismatch factor uncertainty [eq (2)], a generator of normally distributed random numbers was then used to simulate possible impedances around the average obtained earlier. This was done for 100 samples and with several iterations. We then calculated the reflection coefficients from the generated impedances and input these into the mismatch equation, an example of which is given by eq (2). The standard deviations from two different ports were then combined using root sum of squares to obtain the final value used in computing the uncertainty in the mismatch factor. After running several simulations, the largest value in the uncertainty was used as the final value, which is

$$\frac{u_{T_x(M/M)}}{T_x} = 0.443\ \%. \tag{9}$$

5.4 Asymmetry

The asymmetry is defined as the ratio of efficiencies η_s/η_x appearing in the radiometer equation (1). Its contribution to the uncertainty in the measured noise temperature is

$$\frac{u_{T_x}(\eta/\eta)}{T_x} = \left|1 - \frac{T_a}{T_x}\right| u_{\eta/\eta}, \tag{10}$$

where we have used $\mathscr{E}_{\eta/\eta} \approx u_{\eta/\eta}$.

The asymmetry for the NFRad system was measured with a vector network analyzer and utilized the reflective termination (RT) method developed by Daywitt [11-13]. The waveguide systems use a manual asymmetry measurement [2] to determine the actual asymmetries, and then the ratio is calculated. In this approach, one check standard is measured on one port and another check standard is measured on a second port. The check standards are then switched and both are again measured. The product of the ratios from these two measurements is the asymmetry and should equal unity. The asymmetry measurement for the 30/60 MHz system was to be measured using a vector network analyzer, but no analyzers operating at these frequencies were available. Then, we considered using a manual asymmetry method using two hot standards and the ambient, but the measured devices need to be tuned to the DUT's impedance. Since we cannot tune a noise source/diode, there will be a mismatch for one of the DUTs in the measurement. In order to determine the absolute uncertainty, we measured the two standards without matching the ambient standard to either of them. The ambient standard was then tuned to one of the standards, the DUTs were measured, the ambient standard was then tuned to the other DUT and measurements were again taken. The two final measurements involved tuning the ambient standard to one DUT during the first half of the measurement and tuning the ambient standard to the other DUT during the second half of the measurement. This process was repeated but the roles were reversed. The mean and standard deviation were computed for each measurement and a final mean and standard deviation were computed for all the sets. This standard deviation was used as the uncertainty in the asymmetry uncertainty. The random uncertainty for several asymmetry measurements was 0.000237, so the total uncertainty in asymmetry is

$$\frac{u_{T_x(\eta/\eta)}}{T_x} = 0.023\ \%. \tag{11}$$

5.5 Other Type-B Uncertainties

The measured powers enter the radiometer equation through the ratios $Y_x \equiv p_x/p_a$ and $Y_s \equiv p_s/p_a$ in the factor $Y = (Y_x - 1)/(Y_s - 1)$. The powers are measured in the same way as with all other NIST radiometers so the uncertainty analysis is the same, where

$$\frac{u_{T_x}(Y)}{T_x} \le \left|1 - \frac{T_a}{T_x}\right| \times 0.04\ \%. \tag{12}$$

This is negligible unless $T_a \ge 3T_x$.

Although there is no isolator in this system, we must still consider the noise contribution from the preamplifier. This involves calculating the uncertainty in the effective temperature T_e of the source [4, 5]. This equation is given by

$$NT_e = T_1 + T_2 |\Gamma_{2i} - \beta|^2, \tag{13}$$

where T_1 and T_2 are related to the uncorrelated and correlated parts of the noise from the amplifier and β is a complex constant, experimentally determined for each amplifier. The reflection coefficient Γ_2 is the reflection coefficient looking back into the system from the amplifier,

$$\Gamma_{2i} = S_{22} + S_{12}S_{21}\Gamma_i. \tag{14}$$

The S-parameters are for the transmission line, connecting the DUT or test standard, *i*, to the preamplifier, and the subscript *i* denotes the reflection coefficient of device *i*.

By looking at the change in the effective temperature from source *i* to source *j* we obtain

$$\Delta NT_{eij} = 2T_2 Re\, S_{12}S_{21}(S_{22}^* - \beta)(\Gamma_i - \Gamma_j), \tag{15}$$

so that the corresponding DUT error becomes

$$\begin{aligned}\Delta T_x = 2T_2 [((T_x - T_a)/(T_s - T_a))\ & Re S_{12}S_{21}(S_{22}^* - \beta)(\Gamma_s - \Gamma_a) \\ & + Re S_{12}S_{21}(S_{22}^* - \beta)(\Gamma_a - \Gamma_x)].\end{aligned} \tag{16}$$

Because the standards have been tuned to the impedance of the DUT, the reflection coefficients of source *i* and source *j* are the same. In eq (16), ΔT_x is equivalent to zero, but even for small differences in reflection coefficients between devices, ΔT_x is small. These small contributions are accounted for in the mismatch and asymmetry uncertainties.

The uncertainty due to frequency offset and broadband mismatch is the same as that in reference [8],

$$\frac{u_{T_x}(BBMM)}{T_x} = \frac{200\%}{\sqrt{3}}\left|\cos\left(\frac{4\pi f_{IF} l}{30}\right) sinc\left(\frac{\pi B l}{15}\right) - 1\right| \times (|\Gamma_s \Gamma_{r,s}| + |\Gamma_x \Gamma_{r,x}|)\left|1 - \frac{T_a}{T_x}\right|, \qquad (17)$$

where f_{IF} is 0 for NFRad, $B = 0.000773$ at 30 MHz, and $B = 0.00138$ at 60 MHz are the bandwidths in GHz, and $l = 11.43$ is the physical length in centimeters from the input port to the beginning of the first amplifier in the radiometer. The broadband mismatch uncertainty is negligible.

The linearity of the IF section is tested as in previous systems. For each noise temperature measurement, 25 readings are taken with a 3 dB attenuator switched in the IF section of the system, and 25 readings are taken without the attenuator. The two resulting noise temperatures must agree to within 0.2 %. This is taken to be the maximum or expanded (k = 2) uncertainty, leading to a standard uncertainty of

$$\frac{u_{T_x}(lin)}{T_x} = 0.10\ \%. \qquad (18)$$

5.6 Type-A Uncertainty

In noise-temperature calibrations using the present system, we repeat measurements on two different levels. Typically, we make one measurement of the check standard's noise temperature on the DUT port and three separate readings of the DUT on the DUT port. For each of these measurements we take 50 readings (25 each with and without the 3 dB attenuator in the

IF section) of the delivered powers from the two standards and from the check standard or DUT. A noise temperature of the device is computed for each power reading. Thus, in a typical calibration of a customer's DUT, we have three separate groups of 50 measurements, for a total of 150 values of the noise temperature, which are combined to obtain the final value for the measured DUT noise temperature. The question of how to evaluate the type-A uncertainty in obtaining the average value from the multiple measurements was addressed in Section 3.10 of reference [8] for a more complicated measurement scheme. We follow that treatment here, simplifying as appropriate.

We use T_{ij} for the value of a single reading of the noise temperature. The index i denotes the number of the measurements and runs from 1 to N_M (typically 3); the index j denotes the reading number and runs from 1 to N_R (typically 50). We assume that the number of readings N_R is the same for each measurement. We use T_i to denote the mean of the N_R readings for each measurement and use s_i for the associated standard deviation:

$$T_i = \frac{1}{N_R}\sum_{j=1}^{N_R} T_{ij},$$
$$s_i^2 = \frac{1}{(N_R - 1)}\sum_{j=1}^{N_R} (T_i - T_{ij})^2, \tag{19}$$

where T and s are the mean and standard deviation of the N_M measurements:

$$T = \frac{1}{N_M}\sum_{i=1}^{N_M} T_i,$$
$$s^2 = \frac{1}{(N_M - 1)}\sum_{i=1}^{N_M} (T_i - T)^2. \tag{20}$$

To develop the general expression for u_A we model [14] the variable T_{ij} as

$$T_{ij} = \tau + M_i + R_{ij}, \tag{21}$$

where τ is the true value for the noise temperature of the device being measured, M_i is a random variable representing variations from measurement to measurement (i), and R_{ij} is a random variable that varies with the reading j and the measurement i. Our estimate of the true value is the mean of all readings:

$$\tau \approx T \equiv \frac{1}{N_M N_R} \sum_{i=1}^{N_M} \sum_{j=1}^{N_R} T_{ij}, \tag{22}$$

which is also equal to the mean of the N_M separate measurements. The means of the two random variables are both zero, and their variances will be denoted by

$$\begin{aligned} \langle M_i^2 \rangle &= v_M, \\ \langle R_{ij}^2 \rangle &= v_R, \end{aligned} \tag{23}$$

where the averages are over all indices. The variances can be estimated from the measured values T_{ij} by

$$\begin{aligned} \frac{1}{N_M(N_R - 1)} \sum_{i,j} (T_{ij} - T_i)^2 &\approx v_R, \\ \frac{1}{(N_M - 1)} \sum_{i} (T_i - T)^2 &\approx v_M + \frac{v_R}{N_R}. \end{aligned} \tag{24}$$

The equalities are only approximate because we are dealing with a limited sample. We can solve eq (24) for v_R and v_M, and use eqs (19) and (20) to write

$$\begin{aligned} v_R &= \langle s_i^2 \rangle, \\ v_M &= s^2 - \frac{v_R}{N_R}, \end{aligned} \tag{25}$$

where the averages are over all free indices and where it is understood that if a negative value

results for v_M it is taken to be 0. The Type-A uncertainty in the determination of $\tau \approx T$ is then the square root of the variance in T,

$$u_A \approx \sqrt{\frac{v_M}{N_M} + \frac{v_R}{N_M N_R}}. \tag{26}$$

Comparison to eq (25) reveals that eq (26) is equivalent to $u_A^2 = s^2 / N_M$, provided that eq (25) does not result in a negative value for v_M. This is as it should be: if we did enough independent measurements to determine s^2 well, that would be sufficient, since it includes the variations from one reading to another. Since we make three separate measurements, we supplement that information with the measured s_i^2.

5.7 Combined Uncertainty

The type-B standard uncertainty for a single noise temperature measurement is obtained by forming the square root of the sum of the squares of the individual contributions eqs (5), (7), (9), (11), (12), (17), and (18),

$$u_B = [u_{T_x}^2(Cry) + u_{T_x}^2(amb) + u_{T_x}^2(Y) + u_{T_x}^2(M/M) + u_{T_x}^2(\eta/\eta) + u_{T_x}^2(BBMM) + u_{T_x}^2(lin)]^{\frac{1}{2}}. \tag{27}$$

In calibrating a customer's device, we make several measurements of its noise temperature. Because the uncertainty defined by eq (27) depends on the measured noise temperature and on various measured reflection coefficients, it is in principle different for each of the separate measurements of the device's noise temperature. In practice, however, there is little difference between the values, and so we use the maximum.

The expanded (k = 2) combined uncertainty is computed from eqs (26) and (27),

$$U_{T_x} = 2\sqrt{u_A^2 + u_B^2}\,. \tag{28}$$

The expanded uncertainty varies with the device being tested, the frequency, and the method of measuring the asymmetry. A typical value for a Type-N source with high noise temperature (above a few thousand kelvins) would be about 1 %. Sources with other coaxial connectors would be measured through adapters and the uncertainty would be somewhat larger.

6. SUMMARY

In this technical note, we have described a tuned radiometer system used to measure noise devices at 30 MHz and 60 MHz. We reviewed the previous system and the improvements and modifications to that system. We also discussed the theory and the testing of the present system. Included were measurement graphs and an uncertainty analysis used to verify the correct operation of the present tuned radiometer.

We thank Andy Terrell for system measurements and Jim Randa for theoretical support.

7. REFERENCES

[1] Counas, G.J.; Bremer, T.H. NBS 30/60 megahertz noise measurement system operation and service manual. Nat. Bur. Stand. (U.S.) IR 81-1656; 1981 December.

[2] Randa, J.R.; Terrell, L.A. Noise temperature measurement system for the WR-28 band. Natl. Inst. Stand. Technol. Tech. Note 1395; 1997 August.

[3] Grosvenor, C.A.; Randa, J.R.; Billinger, R.L. Design and testing of NFRad–A new noise measurement system. Natl. Inst. Stand. Technol. Tech. Note 1518; 2000 March.

[4] Daywitt, W.C. Radiometer equation and analysis of systematic errors for the NIST automated radiometers. Natl. Inst. Stand. Technol. Tech. Note 1327; 1989 March.

[5] Wait, D.F. Radiometer equation for noise comparison radiometers. IEEE Trans. IM-44(2): 336-339; 1995 April.

[6] Larsen, N.T. A new self-balancing DC-substitution RF power meter. IEEE Trans. IM-25(4): 343-347; 1976 December.

[7] Kerns, D.M.; Beatty, R.W. Basic Theory of Waveguide Junctions and Introductory Microwave Network Analysis. Pergamon Press: 89; 1967.

[8] Randa, J. Uncertainties in NIST noise-temperature measurements. Natl. Inst. Stand. Technol. Tech. Note 1502; 1998 March.

[9] Taylor, B.N.; Kuyatt, C.E. Guidelines for evaluating and expressing the uncertainty of NIST measurement results. Natl. Inst. Stand. Technol. Tech. Note 1297, 1994 edition; 1994 September.

[10] ISO Guide to the Expression of Uncertainty in Measurement. International Organization for Standardization; Geneva, Switzerland; 1993.

[11] Daywitt, W.C. Determining adapter efficiency by envelope averaging swept frequency reflection data. IEEE Trans. MTT-38(11): 1748-1752; 1990 November.

[12] Pucic, S.P., Daywitt, W.C. Single-port technique for adapter efficiency evaluation. 45th ARFTG Conference Digest, Orlando, FL, pp. 113-118; 1995 May.

[13] Randa, J.; Wiatr, W., and Billinger, R.L. Comparison of adapter characterization methods. IEEE Trans. MTT-47(12): 2613-2620; 1999 December.

[14] Graybill, F.A. Theory and Application of the Linear Model. Duxbury Press; Belmont, CA; 1976.

Appendix A. TROUBLESHOOTING

Details of the system design are important for troubleshooting purposes and therefore will be covered in this section. We have already covered some basics such as the water-cooled plate and the layout of the equipment, but we discuss the system in depth in this section.

A.1 Placement of Components

The 30/60 MHz system was modified to improve system reliability and performance. In the old setup, most system components, prior to the last amplifier, were not secured to a solid surface and some were almost floating in air due to space limitations. Although the close proximity of components minimized cable loss, we decided, based on prior experience, that the components should be secured for mechanical stability. Also, in the previous system the bolometer mount and the final amplifier were the only components that were water-cooled. We knew from previous systems that this practice was not adequate to ensure temperature stability, especially for the other amplifiers. In the new system, all components were mounted on a water-cooled brass plate to control the temperature and ensure temperature stability. The brass plate is enclosed in a box and placed into a measurement rack along with the impedance meter, the DVM, and a Type IV power meter manifold (described in Section 4). The front-end switches were mounted in a separate box at the bottom of the rack.

A.2 Preamplifier Placement and Operation

After the rebuild, our first measurements showed standard deviations of approximately 500 K. Knowing that the previous system was capable of measurements with standard deviations of only 20 K, we concluded the system was not working properly. A power meter was used to trace measured powers through the system before and after every device to determine which component was not working properly. These values are given in Table A.1 and can be referenced for future problems should they arise.

Table A.1. Initial power measurements through the 30/60 MHz system.

Measurement Position	Power	Power (dBm)
Check standard	2.9 nW	−55.4
At input to pre-amplifier	1.2 nW	−59.4
At output of pre-amplifier	4.0 μW	−24.0
After 30 MHz filter	1.3 nW	−59.0
After IF attenuator	1.2 nW	−59.2
After 5 dB attenuator	490.0 pW	−63.0
After first 30 dB amplifier	370.0 nW	−34.3
After level-set attenuator	27.0 nW	−45.6

Measurement Position	Power	Power (dBm)
After 5 dB attenuator	8.9 nW	−50.5
After second 30 dB amplifier	8.0 μW	−21.0
After 6 dB attenuator	1.9 μW	−27.2
After last 30 dB amplifier	1.5 mW	1.8
Into bolometer	1.5 mW	1.8

Table A.2. Power measurements after moving the pre-amplifier.

Measurement position	Power	Power (dBm)
At input to pre-amplifier	2.6 nW	−56.0
At input to IF box	10.8 μW	−19.7
Into 30 MHz filter	10.4 μW	−19.9

Earlier we stated that all components in the original system were in close proximity to each other. In the present system, the preamplifier was separated from the switches by a cable approximately 0.7 m in length. A co-worker suggested that the cable length between the switches and pre-amplifier might be too long, resulting in large skin-depth losses. The preamplifier was moved to within 5 cm of the switches. The powers were remeasured at the input to the preamplifier, just after the pre-amplifier and into the 30 MHz filter, and these new values are given in Table A.2. There is a difference of almost 5 dBm at the input to the preamplifier. The small position adjustment of the first amplifier reduced the standard deviations to approximately 20 K.

The pre-amplifier is a high-gain device and therefore if any of the measurement ports are open, one or more stages can be destroyed. Therefore, the program warns the user that power is about to be supplied to the preamplifier and that the user must check to make sure no measurement port is open.

A.3 Wiring from Bolometer Mount to DVM

While trying to rewire this section, we had to combine several old pieces of documentation scattered in different locations. This section was written to avoid the problem in the future. Figure A.1 shows a simplified wiring diagram for the 30/60 MHz system starting from the bolometer output. Pins 1, 2, and 4 are tied together at the output of the bolometer. These connect to pins 6, 7, 19, and 20 on a male 25-pin connector that is wired to a 14-pin socket on a Type-IV power meter card. There are two circuits on this card, which is one of eight cards located in the power meter manifold. Our card is in slot 5. From the card, three wires run to an output 25-pin connector. Pin 6 is run to the negative side of the DVM, pin 18 to the positive side of the DVM, and pin 19 is a common ground. We have labeled the diagram using six-port diagram notation to avoid confusion.

A.4 Repair of Ambient Standard

The tuning assembly on the ambient standard became unstable, and during certain movements of the dial, the phase would jump drastically from one reading to another. A decision was made to repair the standard but no complete documentation was available. A brief overview of the repair of the standard is given in this section.

A photograph showing the interior of the ambient standard is shown in Figure A.2. In the photograph one can see both the capacitor-plate structure (the upper photo) and the container that holds the oil and the power resistors that can heat the oil to various temperatures.

The standard was refurbished on May 11, 2001. Upon opening the standard, we found that a gasket had crumbled, allowing oil to seep into the chamber containing the capacitor-plate tuning structure. The old oil from the chamber was replaced with mineral oil and a new gasket was inserted.

A.5 Non linearity of 3 dB Attenuator Measurements

While testing the system, we found consistent readings within the first set of 25 measurements, but there was a noticeable change after removing 3 dB from the path. We concluded that one of the amplifiers was responding nonlinearly to the input signal. The first two amplifiers have low input-power levels on the order of nW (see Table 1), and the last amplifier has an input-power level on the order of a microwatt. We decided that the last amplifier was being saturated, so we tested it and found that it was nonlinear. After replacing this amplifier, the system responded linearly.

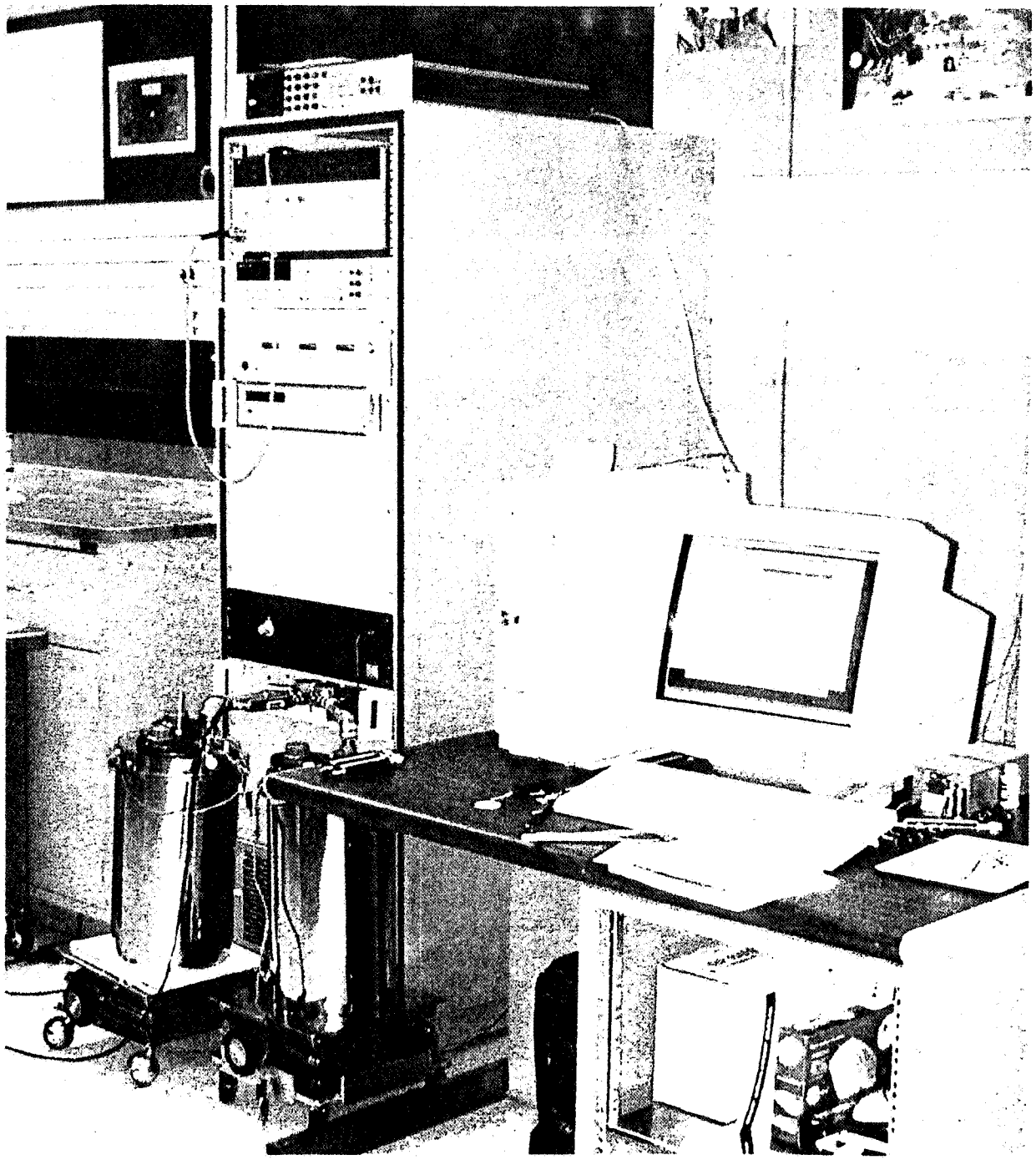

Figure 1. Photograph of complete 30/60 MHz measurement system.

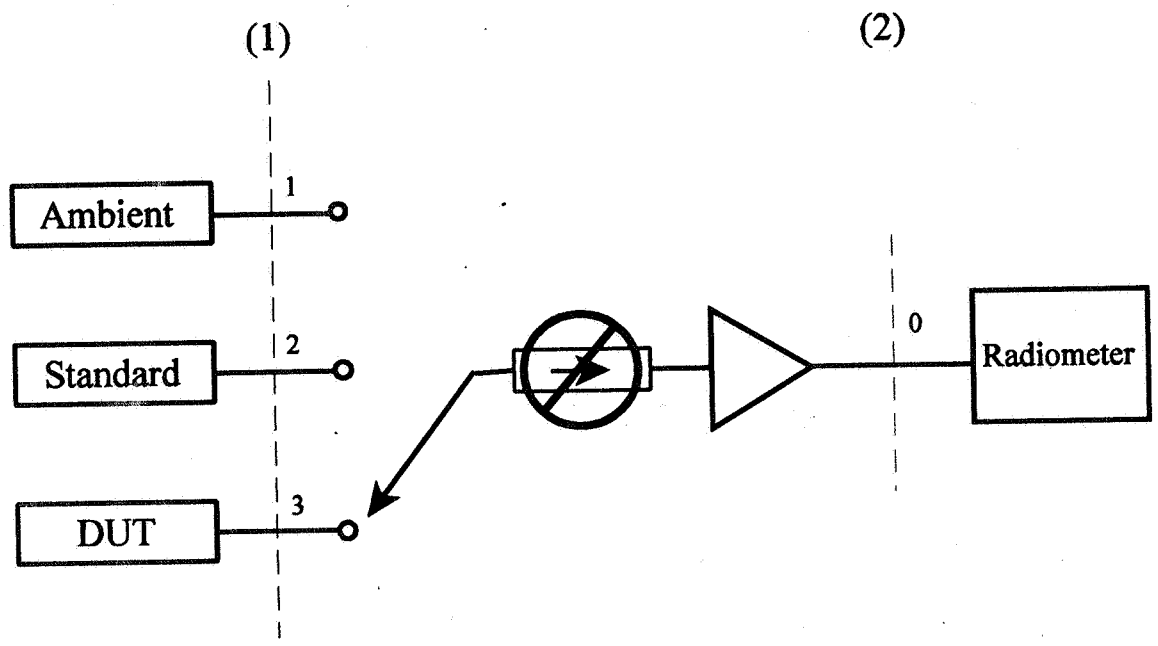

Figure 2. Typical measurement setup.

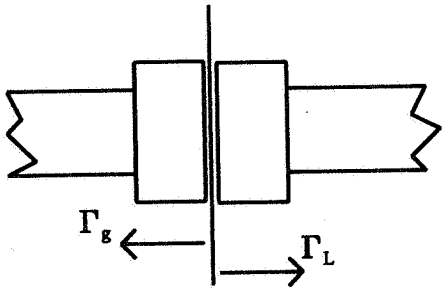

Figure 3. Reflections at any junction giving rise to a mismatch.

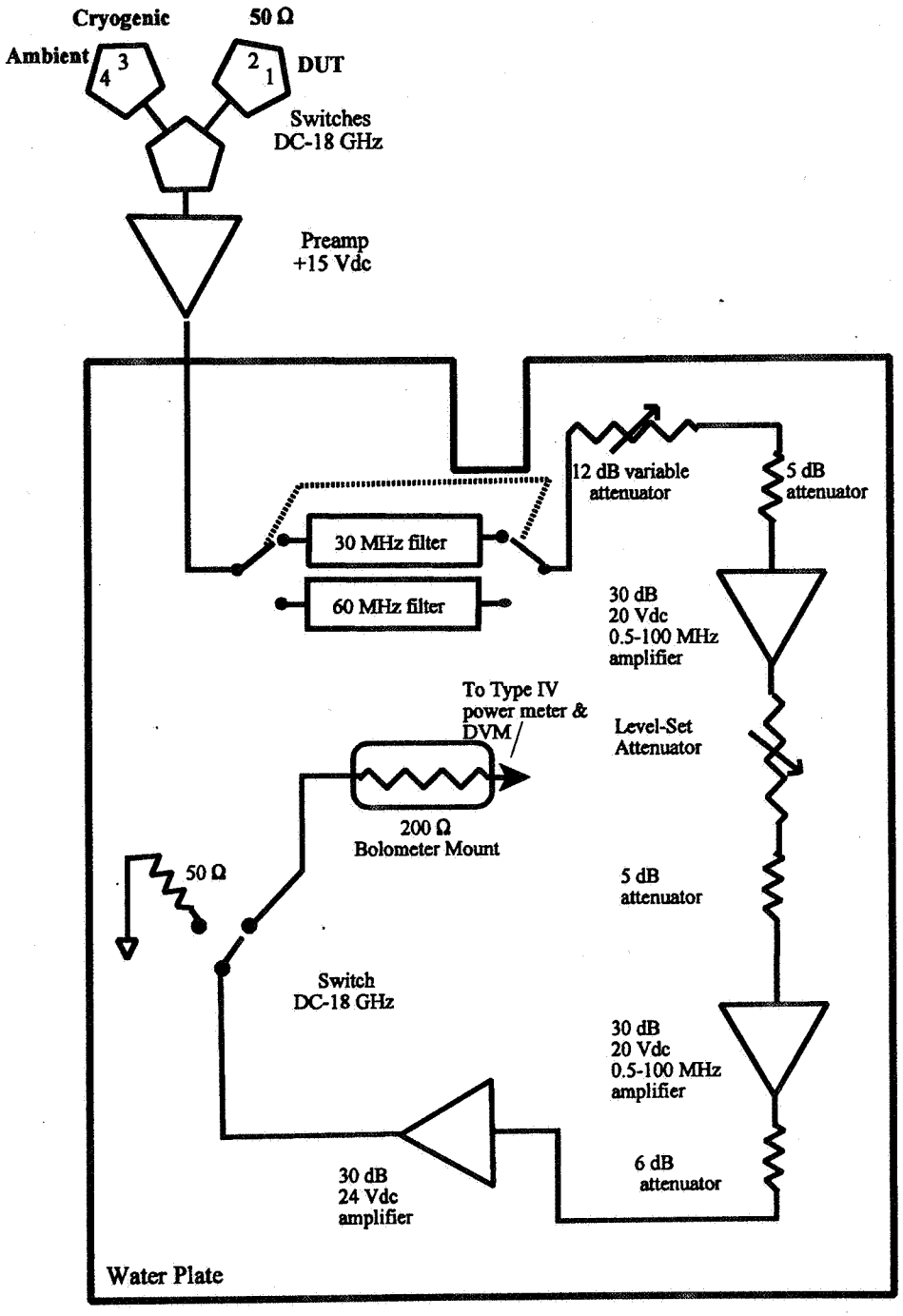

Figure 4. Schematic diagram for 30/60 MHz system.

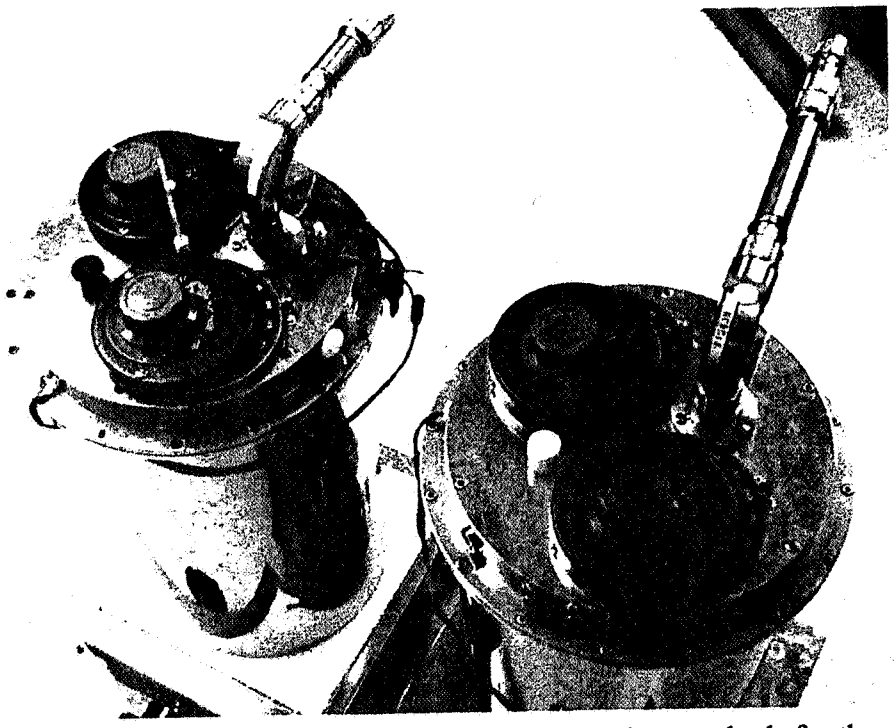

Figure 5. Photograph of cryogenic and ambient noise standards for the 30/60 MHz system.

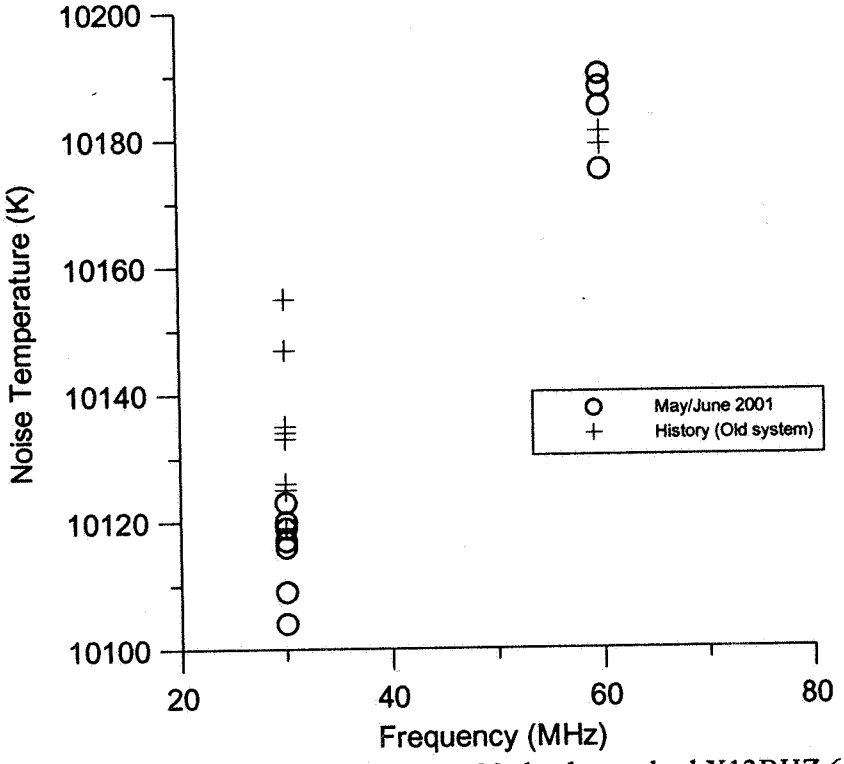

Figure 6. Measurement results for Type-N check standard X13BHZ.617.

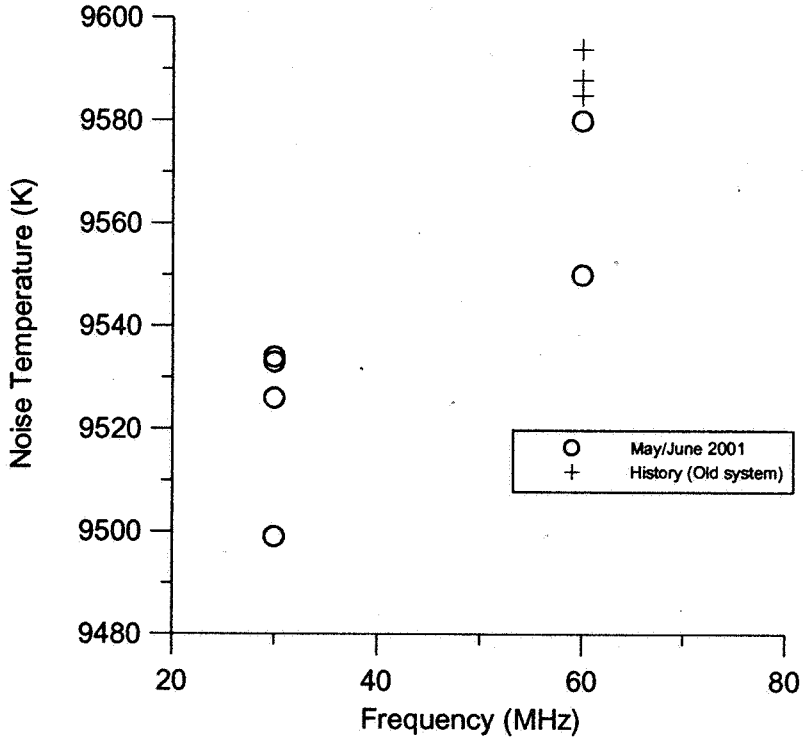

Figure7. Measurement results for Type-N check standard X13BHZ.817.

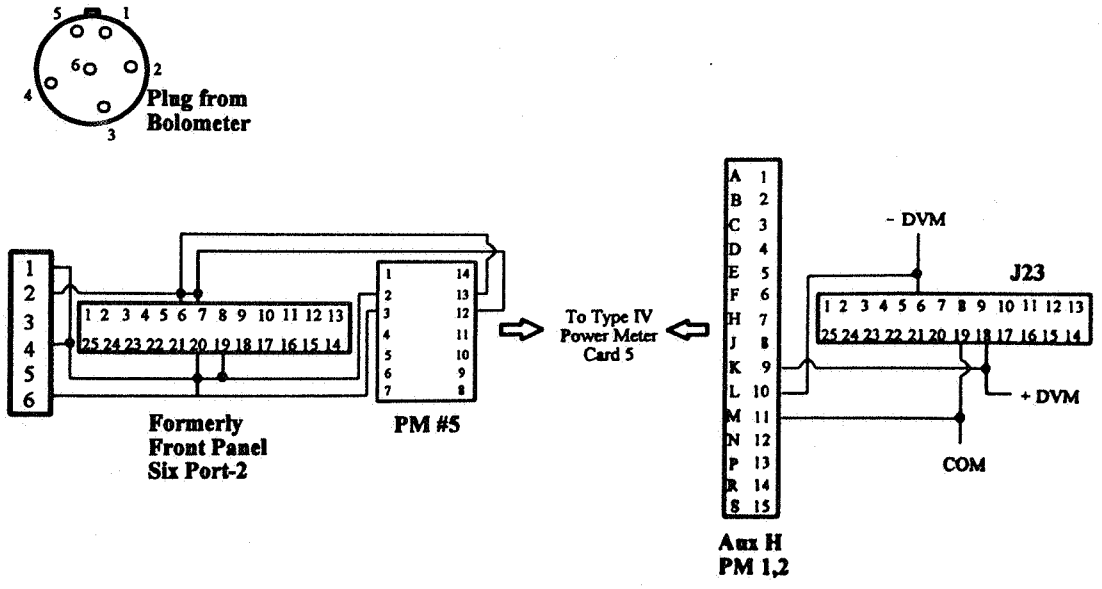

Figure A.1. Wiring diagram for the 30/60 MHz system.

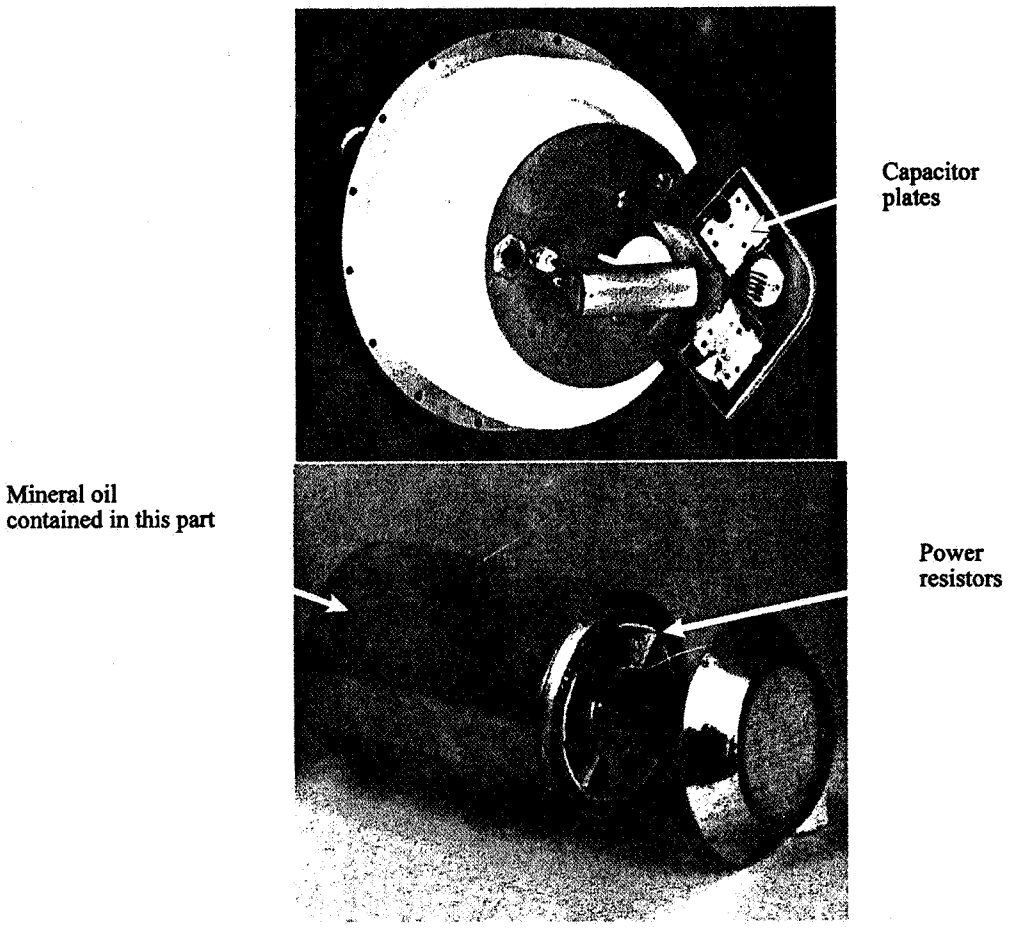

Figure A.2. Photograph of disassembled ambient standard.